

## SILICA-ADDITIONATED CEMENT PASTES OBTAINED FROM DIFFERENT MIXING CONDITIONS: INFLUENCE ON THE HYDRATION PROCESS.

D. ALONSO-DOMINGUEZ<sup>\*†</sup>, A. MORAGUES<sup>†</sup>, E. REYES<sup>†</sup>, I. ALVAREZ-SERRANO\*  
AND C. PICO\*

<sup>\*</sup>CEI Campus Moncloa, UCM-UPM, Madrid, Spain

<sup>\*</sup>Universidad Complutense de Madrid (UCM)  
Facultad de Ciencias Químicas  
Avenida Complutense s/n, 28040 Madrid, Spain  
Email: [ias@quim.ucm.es](mailto:ias@quim.ucm.es) - Web page: <http://www.ucm.es>

<sup>†</sup>Universidad Politécnica de Madrid (UPM)  
ETS de Ingenieros de Caminos, Canales y Puertos  
Calle Profesor Aranguren s/n, 28004 Madrid, Spain  
Email: [amoragues@caminos.upm.es](mailto:amoragues@caminos.upm.es) - Web page: <http://www.upm.es>

**Key words:** Cement paste, silica additive, <sup>29</sup>Si NMR, microstructure, Ettringite

**Abstract:** Several cement pastes with different addition content and size, nano and micro silica, have been prepared, following two different ways in incorporating the additives. Paste test specimens of dimensions 1x1x6 cm have been prepared and characterized by TGA, XRD, SEM and <sup>29</sup>Si NMR. In order to evaluate the rate of hydration, measurements were performed in samples with different curing ages: 2, 7 and 28 days. The obtained results show a higher degree of hydration for previously additivated samples compared to manual mixing cements with the same curing age. Moreover, relevant changes concerning the structure of hydrated compounds have also been detected. The behavior of previously additivated samples is consistent with the presence of hydrated calcium silicoaluminates. Finally, regardless of the method employed, the addition of nanoparticles modifies the size of the obtained crystals. SEM images show a significant reduction in the size of portlandite crystals.

### 1 INTRODUCTION

The use of nanosilica additions in cement-based materials has actually attracted much attention in the last decade. Nanosilica together with several different oxides is among the most employed additions [1,2]. The main searched targets in obtaining new materials depend on the type of nanoparticle chosen. Thus, the addition of nanosilica and nanoalumina mainly aims to improve the characteristic properties of cement paste materials: enhancement of compressive strength, densification of the aggregates/paste

interface, increase of the permeability and therefore optimization of durability, etc [3,4]. Besides this, other additions of metallic oxides concentrate in eventual functional abilities of the material. In this sense, it is worth citing titanium oxide, whose role connected to cement self-cleaning has been widely tested and numerous examples, including specific applications, have been already reported [5]. Iron oxide constitutes another promising additive which concentrates the attention of interesting research concerning the magnetic behavior and possible applications [6]. In all

cases, one of the main difficulties arises for their application due to operational problems associated with the difficulty in workability. In order to optimize the additive efficiency, a good dispersion inside the material is required, and this implies to ensure a good dispersion of particles in the mixing water and a subsequent successful compaction of the material.

The present work reports on the changes produced in the hydration process of cement pastes additivated with nano and microsilica, obtained under different addition methodologies. The main aim deals with establishing the most relevant changes occurring in the hydrated compounds, when comparing mixing methods. In the first method the samples were prepared by means of the dispersion of particles in the mixing water, in the second method the cement is additivated with the silica (nano and micro size).

## 2 EXPERIMENTAL PROCEDURES

### Materials

The plain cement paste (PCP) used as base and reference material is an Ordinary Type I 52.5R Portland cement, which composition is indicated in Table 1. In this work two sets of samples have been studied. One set (denoted AC) consists in samples previously prepared by another research group, for which additions are made directly on the cement. The additivated samples of the second set (denoted as AW), manually mixed samples, were prepared at a water–cement ratio w/c=0.4 using different concentrations of two types of additives: commercial silica nanoparticles (dry powder), supplied by Cab-O-sil® and microparticles (silica fume), supplied by Ferroatlantica SL. In Table 1 the details of their compositions are also gathered. The selected concentrations were, for both sets of samples, 4 and 10 % of nanosilica (denoted with N) and 5 and 10 % of microsilica (denoted with F). In the notation of water manual mixed samples, i.e. AW ones, a “MA” is included at the end of the name in order to avoid ambiguity.

For the AW specimens, the method

employed is a variation of that described in the UNE-EN 196-1: 2005 norm [7], using 60 hits in a compacting unit. The samples were cast into 1×1×6 cm prisms using steel moulds, where they stayed for 24 h in a chamber at 20 °C and 100% humidity. Then they were unmoulded and introduced again into the chamber until the desired curing age: 2, 7 and 28 days. After the required time, the samples were removed and soaked in isopropanol for 24 hours, and after in a stove at 40°C for 24 hours, in order to stop the hydration. The characteristics and notation of the studied samples are indicated in Table 2.

**Table 1:** Composition of employed materials  
(\*Loss on ignition percentage).

Analyte (%)	Portland Cement CEM I 52.5R	Silica Fume	Nanosilica cab-o-sil®
SiO <sub>2</sub>	19.20	95.37	99.9
Al <sub>2</sub> O <sub>3</sub>	6.07	0.34	0.05
Fe <sub>2</sub> O <sub>3</sub>	1.70	0.16	0.003
CaO	63.41	0.08	
MgO	2.56	0.04	
SO <sub>3</sub>	3.38	0.15	
K <sub>2</sub> O	0.82	0.30	
Na <sub>2</sub> O	0.33	0.18	
TiO <sub>2</sub>			0.03
LOI*	2.09	2.70	1.00

**Table 2:** Mix proportions and notation of specimens.  
Cem: cement, SF:silica fume, NS:nanosilica, W:water,  
SP:superplasticizer

Probes	Cem (g)	SF (g)	NS (g)	W (g)	SP (%)
<b>PCP</b>	450	-	-	180	-
<b>4N</b>	432	-	18	180	-
<b>10N</b>	405	-	45	150	4.8
<b>5F</b>	427.5	22.5	-	180	-
<b>10F</b>	405	45	-	180	-
<b>4NMA</b>	432	-	18	180	-
<b>10NMA</b>	405	-	45	150	4.8
<b>5FMA</b>	427.5	22.5	-	180	-
<b>10FMA</b>	405	45	-	180	-

## -Techniques

The X-ray diffraction (XRD) patterns were registered using a PANalytical X'Pert PRO ALPHA1 apparatus using Cu(K $\alpha$ ) radiation with a wavelength of  $\lambda=1.5418$  Å. Sample preparation consisted in simply grounding a representative piece of the paste and then compacting it manually; therefore, the results can be considered as an average.

TGA/DTA profiles were registered using a Setaram Labsys Evo TGA-DTA apparatus. A total quantity of 50-100 mg of sample was heated at 10°C/min up to 1200°C.

Solid state  $^{29}\text{Si}$  NMR-MAS (Magic Angle Spinning Nuclear Magnetic Resonance) spectroscopy was used to characterize the molecular composition. The experiments were carried out on a Bruker Avance 400MHz spectrometer, with a 9.39 T widebore superconducting magnet, operating at 79.49 MHz, with spin rate of 12KHz, 90° pulse length of 4.5  $\mu$ s.

Scanning electron microscopy (SEM) was performed using a JEOL JSM6335FEG, with resolution of 12 Å. Samples were metallized by covering with Au. Semiquantitative chemical analyses were made from energy dispersive X-ray spectroscopy (EDS).

## 3 RESULTS AND DISCUSSION

### 3.1 X-ray diffraction

The XRD patterns of all samples have been registered at different ages of the hydration process in order to qualitatively check the composition and evolution of the cement pastes[8,9]. Figure 1 shows a representative diffraction pattern for the sample 10N\_28D, compared to the PCP pattern, in which the presence of different indicated phases is detected: alite, belite, portlandite, ettringite, calcite, calcium carbonates hydrates and ferrite. The addition of both nano and microsilica considerably improve the hydration process.

Portlandite maxima decreasing in intensity and enhanced background in the 25-35° 2 $\theta$  range indicate a loss of crystallinity indicative of an increase of C-S-H proportion.

### 3.2 TGA/DTA

The TGA/DTA curves have been quantitatively analyzed considering the three typical contributions corresponding to the reactions occurring in the cement-based paste when subjected to a progressive temperature increase (from 40 °C to 1100 °C).

The first endothermic peak is normally attributed to the dehydration of the gel phase (C-S-H), corresponding to the mass loss on the TG profile below ca. 400 °C. Such a peak (rather a broad band) is actually obtained in the AC cement specimens around 130 °C.

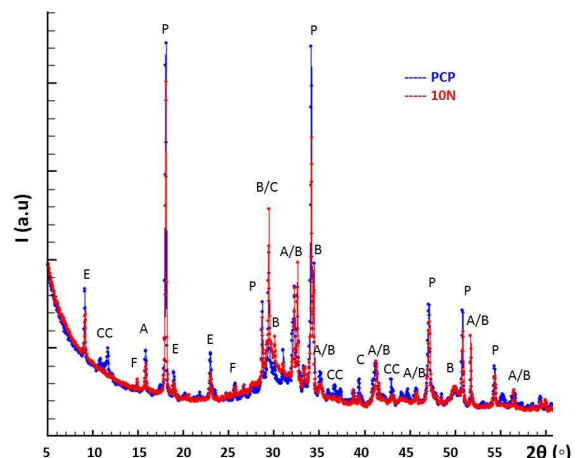


**Figure 1:** XRD patterns of PCP and 10N at curing age of 28 days. E: ettringite, A:alite, B:belite, P:portlandite, F:ferrite, C:calcite, CC: carbonatehydrate

However, in the manual mixing cements, this peak is split in two components, similarly to that found in the cement paste taken as reference, at temperatures around 120 and 180 °C. In them, the first component can be ascribed to the de-hydration of C-S-H gel, whereas the second one could be attributed to de-hydration of ettringite (AFt) or monosulfate (AFm). Figure 2 shows the DTA/TG curves for two selected samples, 10FMA and 4N at 28 days, together with the plain cement paste (PCP) curve, showing both specific features

mentioned above, are presented. These differences obtained in the first step could be ascribed to the stabilization of two different compositions of C-S-H phases; indeed, the incorporation of aluminum to the silica chains giving rise to aluminosilicate structures seems to be favored in the case of AC samples, while in the manual mixed specimens only silica chains are detected. In this sense, the mixing condition influences in a relevant way the tendency towards aluminum isomorphical substitution [10,11].

The second step is also endothermic and corresponds to the de-hydration of calcium hydroxide, resulting in a new loss in mass starting at about 410 °C. A third stage was found around 800 °C, which could be related to minor uncontrolled carbonation of the sample.

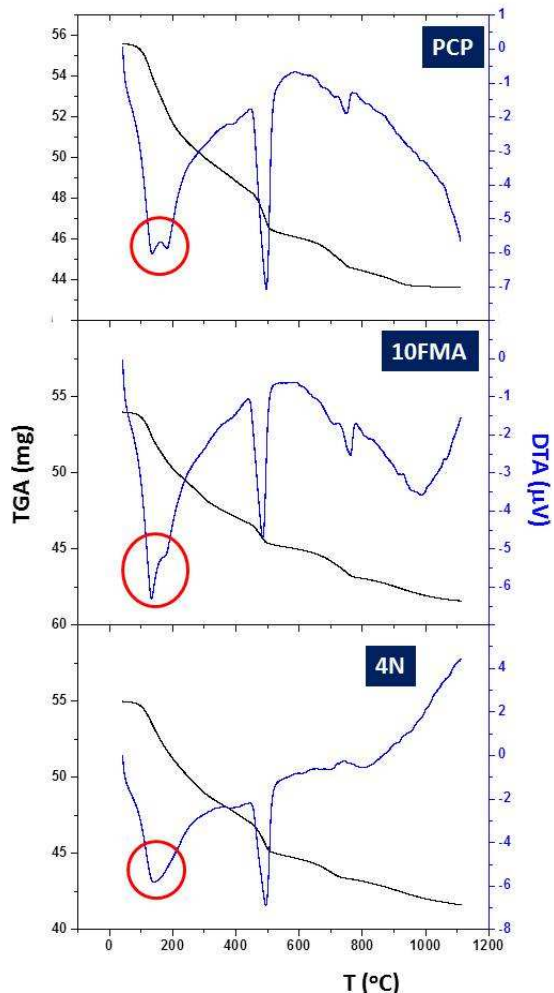


**Figure 2:** TGA/DTA curves for PCP, 10FMA-28D and 4N\_28D. Red circles indicate the bands concerning the first steps.

In order to analyze the evolution of the hydration process, in Figure 3 the hydration degree and the C-S-H loss water mass percentage for all the samples is shown at curing ages of 7 and 28 days.

From these data several tendencies can be underlined:

-It is observed that, for a given curing age and a given additive composition, the AC samples present an enhancement of the C-S-H phase respect to the AW specimens. In this sense, the AC deposition mixing method improves the samples hydration. It is also observed that for the AW samples the hydration is hindered, obtaining smaller amounts of C-S-H gel and lower degrees of hydration than in the sample used as a reference. This could be related to compaction problems together with a higher water demand of the additives once incorporated, as a consequence of poor homogeneity.

-Among the AC samples, those fabricated from nanosilica additions (N) present higher values of both hydration degree and C-S-H water loss percentages than the microsilica additivated ones (F). This is coherent with the expected behavior as the smaller particle size of nanosilica compared to silica fume promotes an enhanced puzzolanic activity and therefore a higher content of secondary tobermorite is stabilized [12]. Note, for example, that the behavior displayed by 4N (minimum addition of nanosilica) is similar to that corresponding to 10F (maximum addition of microsilica), even at early ages.

### 3.3 $^{29}\text{Si}$ MAS-NMR

Polimerization degree (P) and mean chain length (MCL) have been evaluated from deconvolution of  $^{29}\text{Si}$  MAS-NMR spectra, applying the expressions found in previous literature [13]. Typically, the silicate tetrahedra are denoted as  $\text{Q}^n$ , where Q represents the silicon tetrahedron bonded to four oxygen atoms and n is the connectivity, i.e., the number of other Q units attached to the  $[\text{SiO}_4]$  tetrahedron under study.

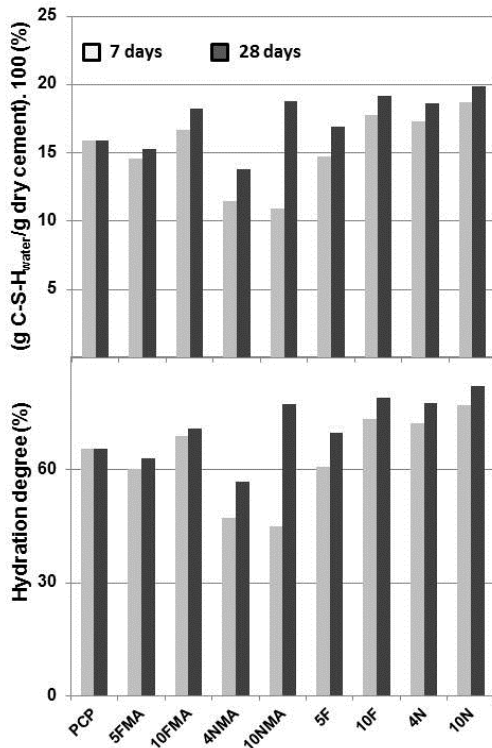


**Figure 3:** Evolution of C-S-H water loss mass and hydration degree for all specimens.

Thus,  $Q^0$  denotes the monomeric orthosilicate anion  $[SiO_4]^{4-}$  (nesosilicate) and typical of anhydrous silicate of cement (C3S and C2S);  $Q^1$  represents an end group of a chain of C-S-H,  $Q^2$  a middle group,  $Q^3$  a chain branching site and  $Q^4$  a three-dimensionally fully cross-linked group both in silica fume and nanosilica. The  $^{29}Si$  nuclei chemical shift ( $\delta$ ) allows obtaining information concerning the organization of tetrahedral links [14-16].

Figure 4 gathers the spectra for 10F\_28D and 4NMA\_28D showing typical bands assignment and a schematic representation of the different chains present, being this fact coherent to that observed from DTA/TGA results discussed above. Tables 3, 4 and 5 include in detail the most relevant parameters for the PCP, 4N and 4NMA samples at different curing ages: chemical shifts (ppm), integral percentages (%), MCL and P (%). In Figure 5 the data for all the samples are graphically gathered with comparative purpose.

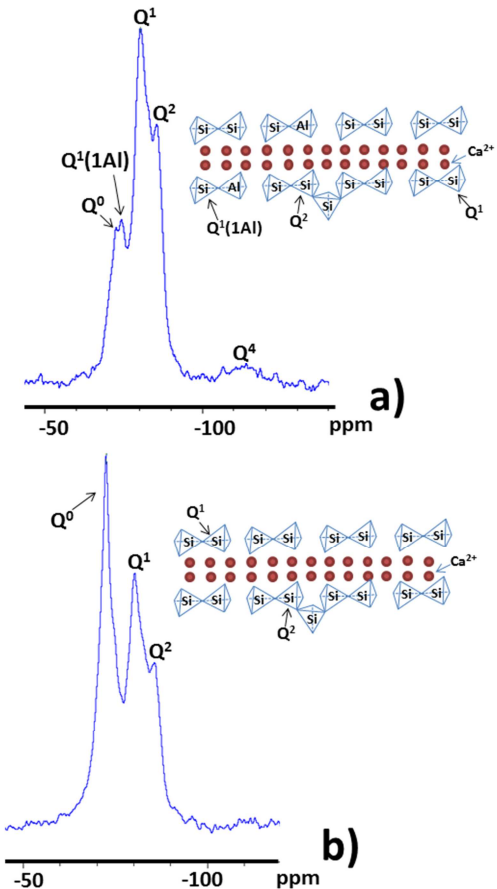


**Figure 4:**  $^{29}Si$  MAS-NMR spectra for a) 10F\_28D and b) 4NMA\_28D. Insets: schemes of the types of C-S-H chains in each case

First, it is observed that in general polymerization values, P(%), are greater for the AC samples than for the manual mixed ones, which indicates that they are more easily hydrated as they present a greater percentage of anhydrous phases (alite and belite), and this is also supported by the thermogravimetric analyses.

**Table 3:** Chemical shifts (ppm), integral percentages (%), MCL and P (%) parameters for PCP.

time signal	2 days		7 days		28 days	
	ppm	I(%)	ppm	I(%)	ppm	I(%)
$Q^0$	-72.9	46.4	-73.0	31.7	-72.9	32.1
$Q^1$	-80.5	42.6	-80.6	39.2	-80.4	51.2
$Q^2$	-85.4	11.0	-85.6	14.9	-85.5	
MCL	2.51		2.56		2.65	
P(%)	53.6		63.0		68.0	

**Table 4:** Chemical shifts (ppm), integral percentages (%), MCL and P (%) parameters for 4N.

time signal	2 days		7 days		28 days	
	ppm	I(%)	ppm	I(%)	ppm	I(%)
<b>Q<sup>0</sup></b>	-72.7	16.9	-72.6	16.4	-73.3	14.1
<b>Q<sup>1</sup></b>	-80.6	51.0	-80.9	53.1	-81.1	39.3
<b>Q<sup>2</sup></b>					-85.4	17.0
<b>Q<sup>1(Al)</sup></b>	-74.5	30.9	-74.0	30.5	-75.1	29.6
<b>Q<sup>4</sup></b>	-110.9	1.2				
<b>MCL</b>	2.00		2.00		2.87	
<b>P(%)</b>	83.1		83.6		85.9	

**Table 5:** Chemical shifts (ppm), integral percentages (%), MCL and P (%) parameters for 4NMA.

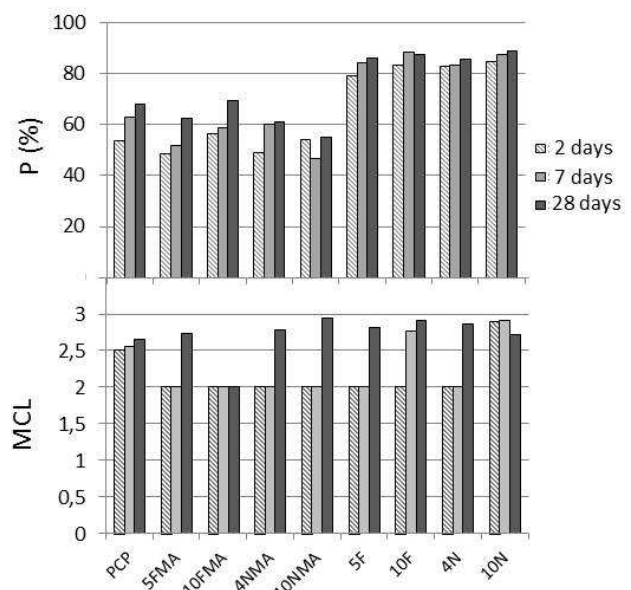
time signal	2 days		7 days		28 days	
	ppm	I(%)	ppm	I(%)	ppm	I(%)
<b>Q<sup>0</sup></b>	-72.5	51.0	-72.7	40.0	-72.7	38.7
<b>Q<sup>1</sup></b>	-80.4	44.6	-80.9	45.9	-80.8	43.9
<b>Q<sup>2</sup></b>					-85.3	17.3
<b>Q<sup>4</sup></b>	-106.9 -111.3	2.6 1.8	-101.0 -107.0 -109.3 -111.9	3.7 3.6 3.8 3.0		
<b>MCL</b>	2.00		2.00		2.79	
<b>P(%)</b>	49.0		60.0		61.3	

Concerning MCL parameter, it has been previously established that C-S-H gel in young pastes consists mainly of dimeric silicate chains (MCL values closer to 2 than to 3) and trimethylsilylation studies have indicated that in older pastes some of the dimers are linked to form pentamers by Q<sup>2</sup> units, Al or Si monomers known as bridging tetrahedra [17].

Comparing microsilica additivated samples prepared differently, it can be observed that the mixing method influences the values of the MCL and P. The AC specimens present greater values of both parameters, which is an interesting result considering that, as it has been previously pointed out [18], there is a lineal relationship between MCL enhancement and the strength compression. The improvement of these parameters could be related to the differences encountered in the obtained C-S-H phase. In the manually mixed

samples no Al signals were detected, which means that no isomorphical Al<sup>3+</sup> substitution in the silicate chains takes place, contrary to that obtained for the AC samples. For these ones Q<sup>1(Al)</sup> signals were present, similar to that found in literature [19], linked to aluminosilicate chains, suggesting that Al substitute Si cations at non-bridging sites; even more, that there are few ions at these sites, i.e. the C-S-H structure is basically constituted by dimers and some pentamers. Thus, Q<sup>2(Al)</sup> signals, typically appearing at ca. -82 ppm [20], are not observed in any specimen and this corroborates that Al<sup>3+</sup> cations are not incorporated at bridging sites. Considering that the Al-containing chains are dimers or trimers there are only two possibilities for the Al<sup>3+</sup> positions: terminal in a dimer or in the middle of a trimer; and this is coherent to the MCL obtained values and the TGA/DTA data.

Comparing nanosilica additivated samples prepared differently, it can be observed that the incorporation of Si in the chains needs a greater curing time in order to be effective (28 days) compared to PCP, but once incorporated it is very efficient; i.e. the elongation of chains does not take place progressively.

**Figure 5:** Evolution of P and MCL with curing age for all the samples.

Some special features are observed in the case of the 10N sample. This sample exhibits great values of MCL since 2 days and therefore it can be assumed that this nanosilica concentration favors a faster chain formation compared to other additions and the reference cement paste. However, although obtained P values are high and follow an expected evolution with curing time, the MCL values smoothly diminish with the curing age from 7 to 28 days. This could be explained in terms of the competition of two growth processes implying Si supply: the C-S-H development and the formation of silica clusters, as previously reported [13]; this would provoke the apparition of new Q<sup>1</sup> signals which enhances the Q<sup>1</sup>/Q<sup>2</sup> ratio, closely related to MCL. Thus, in this sample a large amount of chains is stabilized but they are short. In this sense, high percentages of nanosilica do not improve the MCL values as expected but it rather seems that there is a limit value capable to optimize the formation and growing of long chains.

On the other hand, it is noticeable that a 10% nanosilica addition provokes a faster chains growing than any other else. For instance, the 10N sample shows a high MCL value even at 2 days, whereas this effect is not visible in the 10F specimen. Again, this could be due to the smaller particle size of nanosilica, which permits a higher specific surface and therefore an enhanced puzzolanic activity, giving rise to an increase of C-S-H gel, following the mechanism described by Qing et al. [12].

### 3.4 SEM and EDS

In order to evaluate the microstructure features related to the hydration processes of the samples, SEM and EDS experiments were carried out for all of them. As general features, it is observed that the employed nano and microsilica additions from both tested mixing methods lead to a considerable modification of portlandite crystals and have a great influence on ettringite species.

In Figure 6 SEM images for PCP and

4NMA, at a curing age of 7 days, showing portlandite-type phases are gathered. The composition of CH crystals was confirmed by EDS and a representative spectrum is also show in Figure 6. The portlandite crystal size clearly decreases from 4.2 µm in PCP to 1.4 µm for 4NMA and, interestingly, at the same time the C-S-H phase acquires a denser and more compact aspect [21,22]. This change in morphology and size, together with the homogeneity of dispersion are determinant factors in the improvement of paste compressive strength, making more effective the union between paste and aggregates [23].

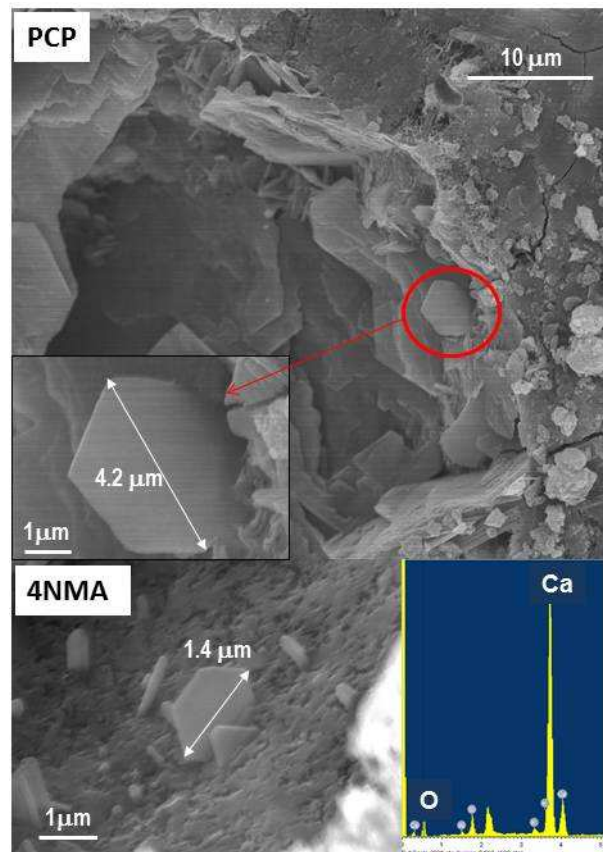


**Figure 6:** SEM images of PCP (up) and 4NMA (left bottom) at a curing age of 7 days; EDS spectrum of CH crystals (right bottom).

For the AC sample with similar additive, 4N, the CH crystal size reduction is also pronounced (from 4.2 µm in PCP to 1.9 µm) and moreover the portlandite crystals lose their crystalline morphology, as it can be appreciated in Figure 7a. Moreover, this type of addition provokes the apparition of a great

quantity of aciculate AFt species, which coat the pores surface, as it can be appreciated in Figure 7b. This process could have a relevant role in aspects such as concrete durability for buildings in marine environments, as the penetration of ions as  $\text{Cl}^-$ ,  $\text{SO}_4^{2-}$ , ... would be prevented [24]. In Figure 7c a micrograph of 4NMA is shown and it can be appreciated that for manual mixing samples with equivalent additive, changes in AFt needles are observed: they are thicker and fewer in number and they do not cover the whole surface.

For microsilica AC additivated samples, portlandite crystals lose crystallinity and are present following fault lines forms, whereas AFt characteristics, i.e. the interior coating of pores, become worse, as it can be observed in Figure 8a. Finally, for the manual mixed ones, the incorporation of microsilica to the gel becomes more difficult as the concentration of additive increases. See, for example, Figure 8b, in which a representative SEM image of the 10FMA sample is gathered. Microstructural characteristics consistent in isolated microsilica spheres are shown. These results are coherent to those obtained from NMR and TGA/TDA, which pointed out low polymerization degrees and small C-S-H percentages, respectively.

#### 4 CONCLUSIONS

Two sets of nano and microsilica additivated cement pastes, prepared by two different mixing methods, have been studied at curing ages of 2, 7 and 28 days. The characterization of the hydration process has been made from XRD, DTA/TG,  $^{29}\text{Si}$  MAS-NMR, EDS and SEM techniques.

It is observed that nanosilica additions provoke higher values of hydration degree than the microsilica ones, coherently with the smaller particle size of the former. The AC deposition mixing method improves the samples hydration, mean chain length and polymerization parameters, and this has been interpreted in terms of different mechanisms implied in each case.

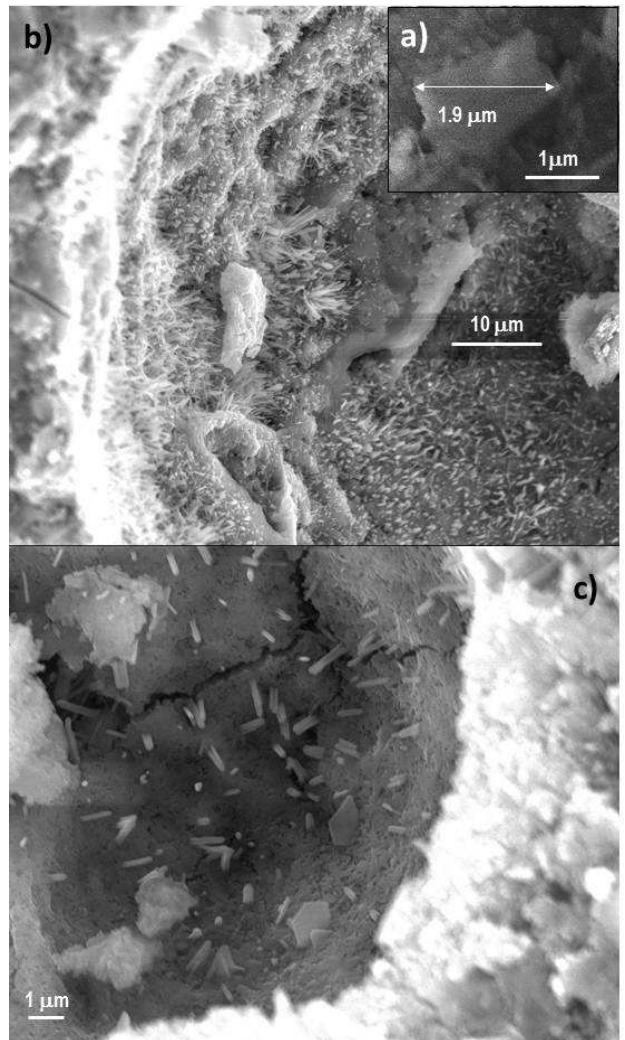


**Figure 7:** SEM images of a) 4N b) and c) 4NMA at the same curing age of 7 days.

In the manually mixed samples no isomorphical  $\text{Al}^{3+}$  substitution in the silicate chains takes place, whereas for the AC samples  $\text{Q}^1(1\text{Al})$  signals prompted to the existence of aluminosilicate chains, in which  $\text{Al}^{3+}$  cations are located in terminal positions of dimers and/or in the middle of trimers, as,  $\text{Q}^2(1\text{Al})$  signals do not appear. New  $^{27}\text{Al}$  NMR experiments are now in route in order to get deeper insight about these structural details.

Finally, it is observed that the employed nano and microsilica additions from both tested mixing methods lead to a considerable modification of the microstructure, especially concerning the morphology of portlandite and ettringite species. Portlandite crystals size is drastically reduced (ca. 60%) when the cement is nanosilica additivated, even with a

concentration as low as 4%. Ettringite is present as needle-type crystals grown inside the pores of the specimens. The deposition type of addition employed in AC samples provokes the apparition of a great quantity of aciculate AFt species efficiently coating the pores surface and therefore leading to promising durability parameters.

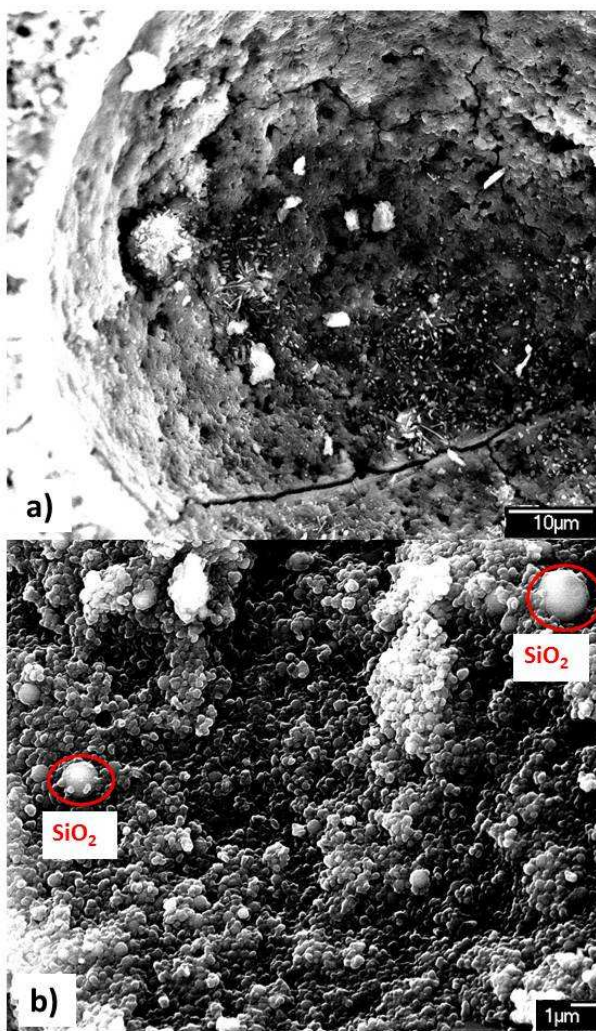


**Figure 8:** SEM images of a) 10F and b) 10FMA at the same curing age of 7 days.

## 5 ACKNOWLEDGEMENTS

We acknowledge financial support from UPM, project BIA2009-14395-C04-04 and from Spanish Ministerio de Educación, Cultura y Deporte, project MAT2010-20117. D. Alonso-Domínguez thanks the CEI Moncloa for the concession of a PhD grant.

Authors are grateful to the CAI centers of UCM (XRD, NMR and electron microscopy).

## REFERENCES

- [1] Singh, L.P., Agarwal, K., Bhattacharyya, S.K., Sharma, U. and Ahlawat, S., 2011. Preparation of silica nanoparticles and its beneficial role in cementitious materials. *Nanomater. Nanotechnol.* **1**:44-51
- [2] Quercia, G., Hüken, G. and Brouwers, H.J.H., 2012. Water demand of amorphous nano silica and its impact on the workability of cement paste. *Cem. Concr. Res.* **42**:344-57.
- [3] Campillo, I., Guerrero, A., Dolado, J.S., Porro, A., Ibáñez, J.A. and Goñi S., 2007. Improvement of initial mechanical strength by nanoalumina in belite cements. *Mat. Lett.* **61**:1889-92.
- [4] Li, Z., Wang, H., He, S., Lu, T. and Wang M., 2006. Investigations on the preparation and Mechanical properties of the nano-alumina reinforced cement composite. *Mat. Lett.* **60**:356-59.
- [5] Ming-Zhi, G., Tung-Chai, L. and Chi-Sun, P., 2012. TiO<sub>2</sub>-based self-compacting glass mortar: Comparison of photocatalytic nitrogen oxide removal and bacteria inactivation. *Build. Environ.* **53**: 1-6.
- [6] Li, H., Xiao, H. and Ou, J., 2004. A Study on mechanical and pressure-sensitive properties of cement mortar with nanophasic materials. *Cem. Concr. Res.* **34**: 435-438.
- [7] UNE-EN 196-1: 2005
- [8] Roncero, J., Valls, S. and Gettu, R., 2002. Study of the influence of superplasticizers on the hydration of cement paste using nuclear magnetic resonance and X-Ray diffraction techniques. *Cem. Concr. Res.* **32**:103-08.

- [9] Seiichi, H., Kazuo, Y. and Hirao, H., 2006. XRD/Rietveld analysis of the hydration and strength development of slag and limestone blendend cement. *J. Adv. Concr. Technol.* **4**:357-67
- [10] Esteves, L.P., 2011. On the hydratation of water-entrained cement-silica systems: Combined SEM, XRD and thermal analysis in cement pastes. *Thermochim. Acta*. **518**:27-35.
- [11] Pane, I. and Hansen, Will. 2005. Investigation of blended cement hydration by isothermal calorimetry and thermal analysis. *Cem. Concr. Res.* **35**:1155-64.
- [12] Qing, Y., Zenan, Z., Deyu, K. and Rongshen C. 2007. Influence of nano-SiO<sub>2</sub> addition on properties of hardened cement paste as compared with silica fume. *Constr. Build. Mater.* **21**: 539-45
- [13] Dolado J.S., Campillo, I., Erkizia, E., Ibáñez J.A., Porro, A., Guerrero A. and Goñi, S. 2007. Effect of nanosilica additions on Belite cement pastes held in sulfate solutions. *J.Am.Ceram.Soc.* **90**:3973-76.
- [14] Masse, S., Zanni, H., Lecourtier, J., Roussel J.C. and Rivereau, A. 1993. 29Si solid state NMR study of tricalcium silicate and cement hydration at hight temperature. *Cem. Concr. Res.* **23**:1169-77.
- [15] Cong, X. and Kirkpatrick R.J. 1996. 29Si MAS NMR study of the structure of calcium silicate hydrate. *Advn. Cem, Bas. Mat.* **3**:144-56.
- [16] Dyson, M.H., Richardson I.G. and Brough R.A., 2007. A combined . 29Si MAS NMR and selective dissolution technique for the quantitative evaluation of hydrated blast furnace slag cement blends. *J.Am. Ceram. Soc.* **90**:598-602.
- [17] Richardson I.G. and Groves G.W., 1997. The structure of the calcium silicate hydrate phases present in hardened pastes of white Portland cement/blast-furnace slag blends. *J. Mat. Sci.* **32**:4793 – 4802.
- [18] Gaitero J.J., Campillo, I and Guerrero A. 2008. Reduction of the calcium leaching rate of cement paste by addition of silica nanoparticles. *Cem. Concr. Res.* **38**:1112-1118.
- [19] Richardson I.G. 1999. The nature of C-S-H in hardened cements. *Cem. Concr. Res.* **29**:1131-1147.
- [20] Rawal, A., Smith, J.B., Athens, L.G., Edwards,L.C., Roberts, L., Gupta, V. and Chmelka, F. 2010. Molecular silicate and aluminate species in anhydrous and hydrated cements. *J. Am.Chem.Soc.* **132**: 7321-37.
- [21] Byung-Wan, J., Chang-Hyun, Kim., Ghi-ho, T. and Jong-Bin, P. 2007. Characteristics of cement mortar with nano-SiO<sub>2</sub> particles. *Constr. Build. Mater.* **21**: 1351-55.
- [22] Björnström J., Martinelli, A., Matic, A., Börjesson L. and Panas I. 2004. Accelerating effects of colloidal nano-silica for beneficial calcium-silicate-hydrate formation in cement. *Chem.Physic.Lett.* **392**:242-48
- [23] Hiu, L., Hiu-gang, X., Yuan, J. and Jinping O. 2004 . Microstructure of cement mortar with nano-particles. *Composites Part B: engineering.* **35**:185-189
- [24] Mahmoud, S., Reyes, E. and Moragues, A. 2010. Evolution of microstructure and mechanical behavior of concretes utilized in marine environments. *Materials and Design* **31**: 3412-3418.